Inter-comparison between the Aerosol Optical Properties Retrieved by Different Inversion Methods from SKYNET Sky Radiometer Observations over Qionghai and Yucheng in China

Zhe Jiang[1], Minzheng Duan[1*], Huizheng Che[2*], Wenxing Zhang[1], Teruyuki Nakajima[3], Makiko HashimotoB[3], Bin Chen[1], and Akihiro Yamazaki[4]

[1]Institute of Atmospheric Physics, Chinese Academy of Sciences, Beijing 100029, China

[2]State Key Laboratory of Severe Weather (LASW) and Institute of Atmospheric Composition, Chinese Academy of Meteorological Sciences (CAMS), CMA, Beijing 100081, China

[3]Earth Observation Research Center (EORC), Japan Aerospace Exploration Agency (JAXA), Tsukuba, Ibaraki 305-8505, Japan

[4]Japan Meteorological Agency, Meteorological Research Institute, 1-1 Nagamine, Tsukuba, Ibaraki 305-0052, Japan

Correspondence to: Huizheng Che(chehz@cma.gov.cn) and Minzheng Duan(dmz@mail.iap.ac.cn)

Abstract. This study analyzed the aerosol optical properties derived by SKYRAD.pack versions 5.0 and 4.2 (referred to as V5.0 and V4.2) using the radiometer measurements over Qionghai and Yucheng in China, two new sites of the sky radiometer network (SKYNET). As V5.0 uses an a priori size distribution function (SDF) of a bimodal log-normal function, the volume size distribution retrieved by V5.0 presented bimodal patterns with a 0.1-0.2 μm fine particle mode and a 3.0-6.0 μm coarse particle mode both over Qionghai and Yucheng. The differences of the volume size distributions between the two versions were very large for the coarse mode with a radius of over 5 μm. The single scattering albedos (SSAs) by V5.0 correlated to SSAs by V4.2 with R= 0.88, 0.87, 0.90, 0.88 and 0.92 at wavelengths of 400, 500, 670, 870, and 1020 nm over Qionghai, respectively. The correlation coefficients were around 0.95, 0.95, 0.96, 0.94, and 0.91 at the five channels in Yucheng. The SSA differences at 500nm between the two versions decreased while AODs increased over both sites. The seasonal variability of the aerosol properties over Qionghai and Yucheng were investigated based on SKYRAD.pack V5.0. The seasonal averaged AOD over Qionghai had higher values in spring, winter and autumn while lower in summer. The AOD averages were commonly higher in summer and spring than in winter and autumn in Yucheng. The lowest seasonal averaged SSAs were both observed in winter in the two sites. The fraction of the fine aerosol particles was much smaller in summer than the other seasons over Qionghai; the volume distribution of the coarse-mode particle in Yucheng had much large values compared to the

fine-mode particle in all seasons.The results can provide validation data in China for SKYNET to continue improving the data-processing and inversion method. The results provide valuable references for continued improvement of the retrieval algorithms of SKYNET and other aerosol observational networks.

1 Introduction

Aerosols are well known to have significant impacts on climate change and global hydrologic cycle by absorbing, scattering, and reflecting solar radiation (Hansen et al., 1997; Sun et al., 2017) and participating in cloud processes (Ackerman et al., 2000; Ramanathan et al., 2001; Kaufman et al., 2005; Li et al., 2011; Bi et al., 2014; Zhao et al., 2018a). Aerosols also adversely influence human health and visibility (Samet et al., 2000; Pope lii et al., 2002; Yang et al., 2015; Wang et al., 2017). Aerosol-related problems have drawn a great deal of attention (Cai et al., 2016).

Using a sun/sky radiometer to measure both direct solar beam and angular sky radiance is the most common method for a reliable and continuous estimate of detailed aerosol properties over mega-cities around the world. Several aerosol ground-based observation networks were established to understand the aerosol optical properties, validate the inversion products of satellite remote sensing, and indirectly evaluate their effect on climate (Uchiyama et al., 2005; Takamura and Nakajima, 2004; Nakajima et al., 2007). SKYNET, the focus of this study, is a ground-based research network of using sky radiometers (PREDE Co., Ltd., Tokyo, Japan) with observation sites principally located in Asia and Europe (Che et al., 2014).

The direct solar and angular sky radiance data measured by the sky radiometers are processed to obtain the aerosol optical properties, such as aerosol optical depth (AOD), single scattering albedo (SSA), complex refractive index, and volume size distribution function (SDF) using SKYRAD.pack, which is the official retrieval algorithm of the SKYNET network (Nakajima et al., 1996) having several different versions. SKYNET currently uses the SKYRAD.pack algorithm version 4.2 (Takamura and Nakajima, 2004). The aerosol retrievals derived from SKYRAD.pack version 4.2 algorithm have been used to investigate the regional and seasonal characteristics of aerosols for climate and environmental studies and validate satellite remote sensing results (e.g., Kim et al., 2004; Che et al., 2008; Campanelli et al., 2010; Estellés et al., 2012a; Wang et al., 2014; Che et al., 2018). Recently, a new SKYRAD.pack version 5.0 was proposed to improve SSA retrievals (Hashimoto et al., 2012), there are a few applications of SKYRAD V5.0 in China, and it was just preliminarily used to retrieve aerosol optical properties over

Beijing in China (Che et al., 2014).

This study presents the aerosol optical properties over Qionghai and Yucheng by using SKYRAD.pack V5.0 and V4.2 from SKYNET sky radiometer measurements during February 2013 to December 2015. This work is designed to achieve the following objectives: (1) investigate the difference of the aerosol optical properties derived by SKYRAD.pack V5.0 and V4.2 over the two SKYNET sites; and (2) analyze the seasonal variability of aerosol optical properties over Qionghai and Yucheng based on SKYRAD.pack V5.0. The results presented in this study provide valuable references for continued improvement of the retrieval algorithms of SKYNET and other aerosol observational networks.

2 Site description, instrumentation, and inversion method

2.1 Instrumentation

The sky radiometer (Model POM-02, PREDE Co. Ltd.) was deployed at Qionghai and Yucheng from February 2013 and February 2013, respectively. The PREDE-POM02 model was equipped with an InGaAs detector to measure the direct solar irradiance and the sky diffuse radiance at 11 wavelengths, namely, 315, 340, 380, 400, 500, 675, 870, 940, 1020, 1627, and 2200 nm. The data from five channels at 400, 500, 675, 870, and 1020 nm were used here to retrieve the aerosol optical properties over Qionghai and Yucheng. The full angle field of view is 1.0°, while the minimum scattering angle of measurement is approximately 3°. The sky radiance is measured at 24 predefined scattering angles and at regular time intervals. The sky radiometer operates only during daytime and collects data regardless of the sky conditions. Its dynamic range is 10^7. The typical measurement interval of the sky radiance is 10 min. The Improved Langley (IL) plot method is used in this study to determine the temporal and spectral calibration constants for direct intensity (F0) with accuracy of about 1.5–2.5 %, depending on the wavelength (Nakajima et al., 1996; Campanelli et al., 2004). The calibration by IL plot method was made daily, the variation of F0 due to instrumental drift could be quickly spotted, and then appropriate corrections to data can be applied exactly from the period in which the deviation occurred (Campanelli et al., 2004).

2.2 Site description

The Qionghai site of SKYNET (19.23°N, 110.46°E, 24 m a.s.l.), which was located in the eastern part of Hainan Island, was mainly influenced by East Asia monsoons and typhoons. During summer, the dominant wind is from south to southeast, summer monsoon from the South China Sea and West Pacific brought most of the annual rainfall to the island (Zhu et al., 2005), whereas the winter monsoon from

Inner Mongolia carries dry winds to the area (Zhu et al., 2005; Peel et al., 2007; Yin et al., 2002). Annual average rainfall in Qionghai is estimated about 1653.4 mm. Maximum high temperature occurs in July, with monthly average of 28.6 ^{o}C, monthly lowest temperature occurs in January, with monthly average of 19.1^{o}C (Yin et al., 2002).

The other measurement site in this study was located in rural Yucheng (36.82°N, 116.57°E, 22 m a.s.l.), Shandong Province, China, which is almost in the centre of the North China Plain. The selected site is in an open field surrounded by farmland. The region belongs to semi-humid and temperate monsoon climate zone, characterized by a mean annual temperature of 21^{o}C and mean annual precipitation of 610 mm mainly distributed in summer months (Chen et al., 2012).Yucheng and the surrounding areas are famous for their agriculture (e.g., wheat and corn) and grazing land (e.g., donkeys and chickens). In addition, the site near 20 to 30 km radius located several factories in the production of inorganic and organic fertilizers (Wen et al., 2015), and the application of fertilisers to farmland emitted a great deal of NH3 (Zhao et al., 2012). Meanwhile, Yucheng is located in the downwind of the Beijing-Tianjin-Hebei region, long-distance transport of sources of industrial pollution and biomass burning contributed significantly to the concentrations of pollutants in Yucheng (Lu et al., 2016). The major chemical compositions in PM2.5 at the two sites were introduced in Section 3.2.1.

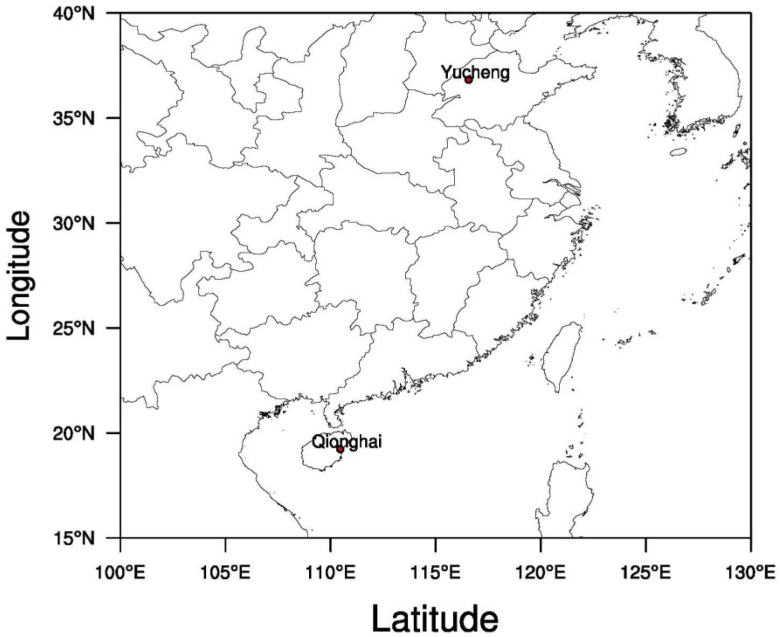

Figure 1: The locations of the two SKYNET sites in the study

2.3 Inversion method

The aerosol optical properties (i.e., AOD, SSA, complex refractive index, and volume SDF) were derived in this study by using SKYRAD.pack V4.2 and V5.0. Within the SKYRAD.pack code, the inversion schemes were used to derive the single scattering term β(Θ) from the measurements of the normalized sky flux R(Θ) and retrieve the aerosol SDF v(r) (as a function of particle radius, r) from data β(Θ) and AOD τ. The inversion of β(Θ) was performed through a non-linear iterative method. Each step of the loop contained the procedure for retrieving v(r) using a constrained linear or a non-linear iterative method. Non-sphericity particle model are neither included in V4.2 nor V5.0.

The retrieved v(r) in each iteration step was used as an input parameter for the radiative transfer model (Nakajima and Tanaka, 1988) to simulate R(Θ), which was compared with the measured R(Θ) to evaluate the root mean square difference ε(R). The maximum number of iterations and the tolerance parameter for the convergence of R were set as 20 and 0.1%, respectively.

The retrieval of v(r) from β(Θ) and τ data in SKYRAD.pack V4.2 was conducted using a constrained linear method. The inversion method consisted of a linear matrix formulation, in which the solution stability was controlled by the requirement that it agrees both with the input data and the imposed weighted constraints (Nakajima et al., 1983).

$$f = Kx + \varepsilon. \quad (1)$$

where f is the vector of the β(Θ) and τ data, and x is a state vector containing the values of size distribution vi = $v(r_i)$ with r_i equidistant on a logarithmic scale (i.e., $\ln(r_{i+1}) - \ln(r_i) = \text{const}$). The components of vector ε were the error of each datum, K = K (m(λ)), a matrix of the kernel coefficients calculated for the fixed values of the complex refractive index (m(λ)).

V4.2 used the iterative relaxation method of Nakajima et al. (1983, 1996) to remove the multiple scattering contribution and derived an optimal solution using a statistical regularization method (Turchin and Nozik, 1969) by minimizing the following cost function as proposed by Phillips (1962) and Twomey (1963):

$$e^2 = |(f - Kx)|^2 + \gamma |Bx|^2. \quad (2)$$

where B is a smoothing matrix used to generate a priori information that forces the solution x to be a smooth function of ln(r); and γ is a Lagrange multiplier coefficient to minimize the first term of the right-hand side of Eq. (2). The solution of Eq. (1) provided a smooth retrieval of the size distribution v(r) corresponding to the minimum of e2 defined by Eq. (2). In such an approach, both the solution v(r) and e^2 depended on the assumed value of the complex refractive index m(λ). The complex refractive index m(λ) in each iteration was also evaluated together with v(r), but the retrieved m(λ) can only be chosen from the predefined set of values.

The m(λ) values in SKYRAD.pack V5.0 were directly included in the state vector x. Eq. (1) becomes non-linear, and V5.0 solved it using the non-linear maximum likelihood method defined by Rodgers (2000). This method was based on the Bayesian theory.

$$p(x|f) = p(f|x)p(x)/p(f) . \quad (3)$$

where p is the probability density function defined as the Gaussian distribution; and x and f denote the state and measurement vectors, respectively. Accordingly, x was chosen in the maximum likelihood method, such that the posterior probability p(x|f) becomes the maximum under the condition that a priori information is already given. We obtained the following equation in the tangential space to be solved by a Newtonian method by organizing this non-linear equation, such that p(x|f) = max:

$$x_{k+1}=x_k+(U_k^T S_e^{-1} U_k+S_a^{-1})^{-1}[U_k^T S_e^{-1}(f-f_k)- S_a^{-1}(x_k-x_a)] \quad (4)$$

where x_k is the solution at the k^{th} iteration step; $f_k=f(x_k)$ is an observation modeled using x_k ; x_a is the a priori value of x; S_e is the measurement error covariance matrix; S_a denotes the covariance matrix defined by a priori and state values, $S_a=(x-x_a)(x-x_a)^T$; and U is the Jacobi matrix, $\partial f/\partial x$. The retrieval algorithm used in V5.0 allowed a rigorous retrieval of both the aerosol size distribution and the spectral complex refractive index.

The non-linear inversion has a strong dependence on the estimation of the first-guess solution. Version 5.0 uses an a priori SDF of a bimodal log-normal function as follows:

$$v(r) = \sum_{n=1}^{2} C_n \exp\left[-\frac{1}{2}\left(\frac{\ln r-\ln r_{mn}}{\ln S_n}\right)^2\right] \quad (5)$$

where r_{m1} = 0.1 μm; r_{m2}= 2.0 μm; S_1 = 0.4; S_2 = 0.8; $C_1 = 1.0 * 10^{-12}$; and $C_2 = 1.0 * 10^{-12}$, following the reported climate values (Higurashi et al., 2000). For a priori estimates of the refractive index, the real (m_r) and imaginary (m_i) parts were set as m_r = 1.5 and m_i = 0.005, respectively.

SKYRAD V5.0 developed a stricter data quality control method of observation data and cloud screening. The standard process of quality control in SKYNET applies a retrieval error between observations and calculated theoretical values by using retrieval values, σ_{obs}

$$\sigma_{obs} = \sqrt{W_e \sum_i\left(\frac{\tau_{\lambda_i}}{\tau_{\lambda_i}^{meas}}-1\right)^2 + W_p \sum_i \sum_j\left[{R_{\lambda_i}(\Theta_j)}/{R_{\lambda_i}^{meas}(\Theta_j)}-1\right]^2} \quad (6)$$

where ($\tau_{\lambda_i}^{meas}$ and $R_{\lambda_i}^{meas}$) and (τ_{λ_i} and R_{λ_i}) are measured and retrieved observation vectors for the AOD and relative sky radiance, N_i , N_j , and $N_{total} = N_i+N_i\times N_j$ indicate the number of measured wavelengths, scattering angles, and their total, respectively, $W_e= W_P = 1/N_{total}$. In V4.2, the data if the value of σ_{obs} is larger than 0.2, but σ_{obs} is set 0.07 as a threshold for data rejection in V5.0. There are some other differences between V4.2 and V5.0 on the issue of quality control of observation data and cloud screening (Hashimoto et al., 2012).

3 Results and discussion

The results retrieved by SKYRAD.pack V4.2 were used to compare with the results retrieved by SKYRAD.pack V5.0. The inter-comparisons of the volume size distribution, single scatter albedo, and refractive index between V5.0 and V4.2 were based on 1397 measurements for 355 days over Qionghai and 5830 measurements for 473 days over Yucheng. Considering a relatively low retrieval accuracy of SSA when AOD < 0.2 (Dubovik et al., 2000), only the measurements with AOD ≥ 0.2 were selected to be effective values in this study. Figure 2 showed the plots of AOD values at each wavelength derived from the solar direct irradiance between the two versions. High correlation was found with a significant coefficient larger than 0.995 at each band in both sites except 1020nm over Qionghai. High consistency of AODs between V4.2 and V5.0 indicates that the inversion process in V5.0 did not bring about a large change in the retrieved direct solar radiation (Hashimoto et al., 2012).

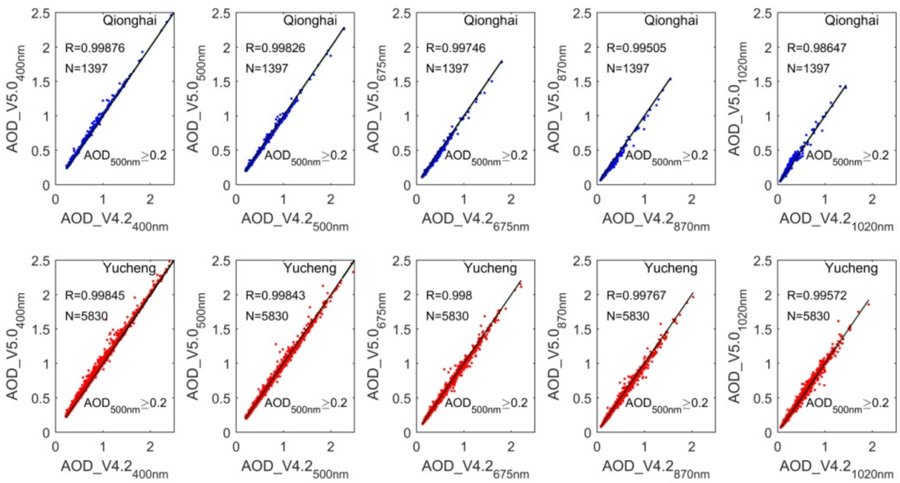

Figure 2: Scattergrams of the aerosol optical depth (AOD) between SKYRAD V4.2 and V5.0 at wavelengths of 400, 500, 670, 870, and 1020 nm over Qionghai and Yucheng during February 2013 to December 2015.

3.1 Inter-comparison of aerosol properties results between SKYRAD V4.2 and V5.0

3.1.1 Inter-comparison of the volume size distribution results between SKYRAD V4.2 and V5.0

Aerosol size properties were one of the most important sources of information for both the observation and modeling of radiative forcing (Dusek et al., 2006). The volumes at each bin were monthly averaged during the experiment period, for V4.2 and V5.0 over Qionghai and Yucheng (Figure 3).The SDF by V4.2 usually showed a predominant peak at the coarse mode with a radius over 10 μm. In Qionghai, the SDF by V4.2 showed a slightly tri-model pattern in February. There were tri-model patterns with three peak volumes at radius of 0.026μm, 0.25μm, 16.54μm and 0.25μm, 1.69μm, 11.31μm in volume SDF by V4.2 in August and September over Yucheng, respectively. As V5.0 uses an a priori SDF of a bimodal log-normal function (Hashimoto et al., 2012), the volume SDF derived by V5.0 generally showed the classic bi-mode patterns at both Qionghai and Yucheng. The SDF from V5.0 showed two peaks at radii of 0.17μm and 5.29μm over both sites. Generally, the SDF retrieved by V4.2 was similar to V5.0 at radius < 5 μm. The large differences in volume SDF at radius over 5 μm between V4.2 and V5.0 were mainly related to that the smoothness condition in V4.2 given by Eq. (2) allowed the retrieved SDF to be distributed beyond 10 μm radius, whereas the strong constraint on the SDF for the coarse mode particles as shown in Eq. (5) was applied in V5.0 (Hashimoto et al., 2012).

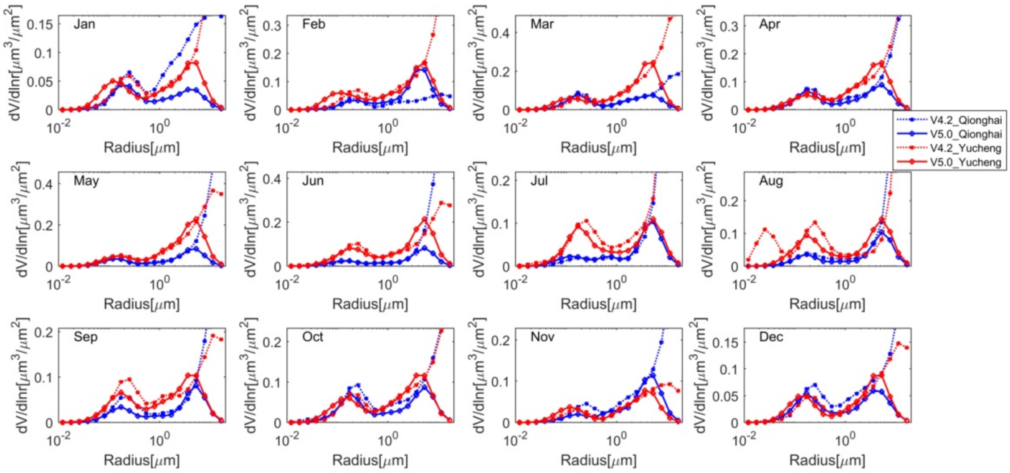

Figure 3: Retrieved monthly volume size distribution between SKYRAD V4.2 (dotted lines) and V5.0 (solid lines) for Qionghai (blue lines) and Yucheng (red lines) during February 2013 to December 2015

3.1.2 Inter-comparison of the single scatter albedo results between SKYRAD V4.2 and V5.0

As a key variable in assessing the climatic effects of aerosols, the SSA is defined as the ratio of the scattering coefficient and the extinction coefficient. It characterized the absorption properties of aerosols and an important quantity in evaluating aerosol radiative forcing. The SSA value is mostly dependent on the shape, size distribution, and concentration of the aerosol particles.

Tables 1 and 2 presented average single scattering albedo and refractive index for SKYRAD 5.0 and 4.2 and the differences between the two versions over Qionghai and Yucheng during February 2013 to December 2015, respectively. The percentage differences of SSA between SKYRAD V5.0 and V4.2 at 400, 500, 675, 870, and 1020 nm over Qionghai were −2.10%, −1.41%, −1.28%, −1.49%, and 0.49%, respectively. Over the Yucheng station, the SSA retrieved from V5.0 were approximately 0.03(3.39%), 0.01(1.29%), 0.02(2.52%), 0.03(3.14%), 0.03(3.73%) lower than those from V4.2 at 400, 500, 675, 870, and 1020 nm, respectively.

Figure 4 presented the compared results of SSA between SKYRAD V4.2 and V5.0 at wavelengths of 400, 500, 670, 870, and 1020 nm over Qionghai and Yucheng during February 2013 to December 2015. As shown in Fig. 4, SSAs by V5.0 correlated to SSAs by V4.2 with R= 0.88, 0.87, 0.90, 0.88 and 0.92 at wavelengths of 400, 500, 670, 870, and 1020 nm over Qionghai, respectively. Although the correlation coefficient was highest at 1020 nm in Qionghai, their patterns were more scattered. The SSA values computed from V5.0 had correlation coefficients around 0.95, 0.95, 0.96, 0.94, 0.91 with those from V4.2 at wavelengths of 400, 500, 670, 870, and 1020 nm over Yucheng. Based on the comparison results over the two sites, it is difficult to conclude that SSAs by V5.0 was larger or lower than those by V4.2.

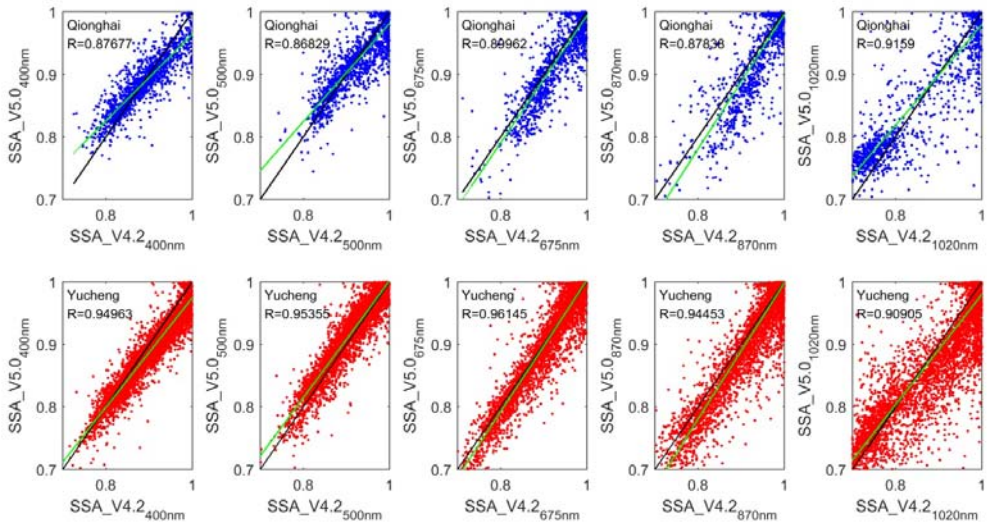

Figure 4: Scattergrams of the single scattering albedo between SKYRAD 4.2 and 5.0 at wavelengths of 400, 500, 670, 870, and 1020 nm over Qionghai and Yucheng during February 2013 to December 2015. Only data with AOD_{500nm}>0.2 are shown. The green line means the fitted linear regression curve.

3.1.3 Inter-comparison of the refractive index results between SKYRAD V4.2 and V5.0

The averaged m_i retrieved from V5.0 at all wavelengths were systemically higher than those by V4.2 over Qionghai (Table 1). The mean values of m_i retrieved from V4.2 were approximately 0.0004, 0.0002, 0.0003, 0.0004, and 0.0001 lower than those from V5.0 for the five channels of 400, 500, 675, 870, and 1020 nm, respectively, over Qionghai. The averaged m_i retrieved by V5.0 was 0.0003, 0.0004, 0.0008 and 0.0004 higher at 400, 675, 870, and 1020 nm wavelengths, respectively, but 0.0002 lower at 500nm, than those retrieved by V4.2 in Yucheng. As shown in Fig. 5, the m_i values by V5.0 were linearly correlated with m_i by V4.2 with R=0.8947, 0.8661, 0.8658, 0.8370, 0.9131 at wavelengths of 400, 500, 675, 870 and 1020 nm in Qionghai. The correlation coefficients between m_i by V5.0 and those by V4.2 at the five wavelengths were all higher than 0.89 over Yucheng.

Generally, the difference in m_r between the two versions was greater than that in m_i (Tables 1 and 2). The mean m_r from V5.0 were approximately 0.03 (2.03%), 0.002 (0.17%), and 0.03 (1.87%) higher, but 0.02 (1.10%), 0.02(1.61%) lower than those from V4.2 over the Qionghai station. The results for m_r showed that m_r at wavelengths of 400, 500, 675 and 870 nm by V5.0 were lower than those by V4.2, but larger than those by V4.2 at 1020 nm over Yucheng. The percentage differences of the mean m_r obtained using the two versions were all within 3.53% both at Yucheng and Qionghai. As shown in Fig. 6, the correlation coefficients between m_i by V5.0 and those by V4.2 at the five wavelengths were all poorer than 0.63 at the two sites.

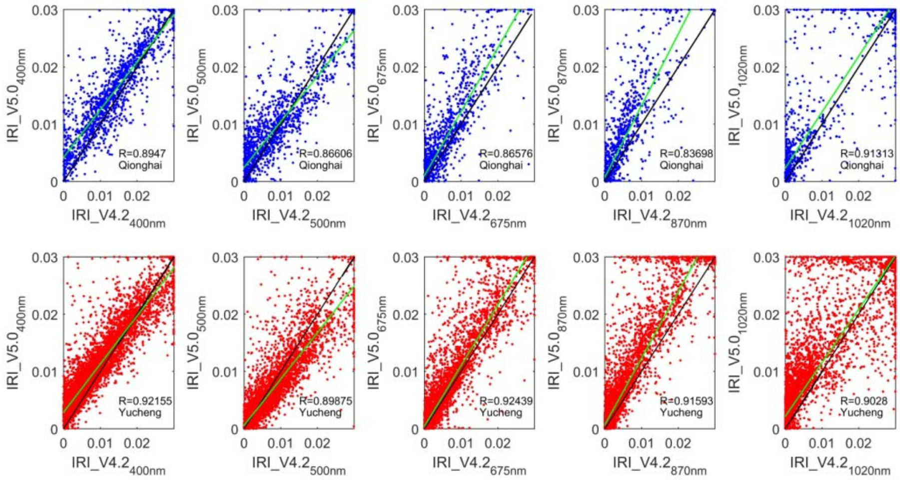

Figure 5: Scattergrams of the imaginary part of the complex refractive index (m_i) results between SKYRAD 4.2 and 5.0 at wavelengths of 400, 500, 670, 870, and 1020 nm over Qionghai and Yucheng during February 2013 to December 2015. The green line means the fitted linear regression curve.

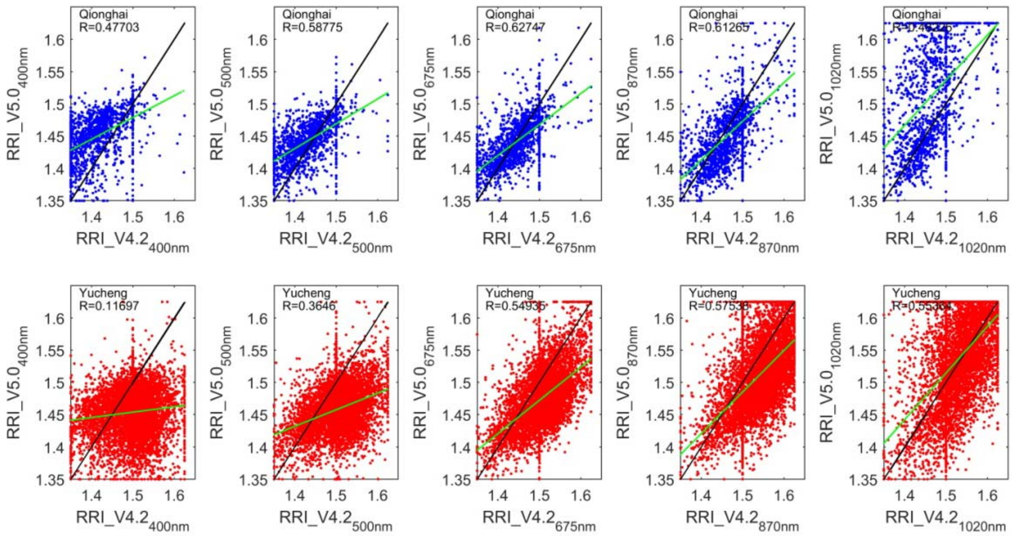

Figure 6: Scattergrams of the real part of the complex refractive index (m_r) results between SKYRAD 4.2 and 5.0 at wavelengths of 400, 500, 670, 870, and 1020 nm over Qionghai and Yucheng during February 2013 to December 2015. The green line means the fitted linear regression curve.

3.1.4 Sensitivity tests for the parameters linked to the SSA differences between the V5.0 and V4.2

Hashimoto et al had performed various test simulations with SKYRAD.pack V4.2 and V5.0

(Hashimoto et al., 2012), they found: V5.0 used an a priori SDF of a bimodal log-normal function, one of the key differences between V4.2 and V5.0 was that V5.0 used a priori estimation, but V4.2 did not; when a large amount of coarse particles of the dust-like aerosol type with radius greater than 10 μm existed , the numerical tests performed by Hashimoto et al showed that V4.2 could retrieve the SDF relatively well, including the coarse mode, in comparison with V5.0, because the smoothness condition given by Eq. (2) allowed the retrieved SDF to be distributed beyond 10 μm radius, on the other hand, V5.0 underestimated the coarse mode of the SDF because of the strong SDF constraint condition given by Eq. (5) with a small model radius r_{m2} = 2.0 μm for the coarse mode SDF (Hashimoto et al., 2012). So we have compared the differences between retrieved SSAs at 500 nm byV5.0 and V4.2 when set r_{m2} = 1.5, 1.8, 2.0(default), 2.5 and 3.0 in Skyrad.pack V5.0 based on the measurements in 2014. As shown in Fig.7, SSAs by V5.0 correlated to SSAs by V4.2 with R= 0.860, 0.837, 0.855, 0.809 and 0.826 when r_{m2} = 2.0(default), 1.5, 1.8, 2.5 and 3.0 in V5.0 over Qionghai, respectively. The SSA values computed from V5.0 had correlation coefficients around 0.940, 0.928, 0.928, 0.921, 0.924 with those from V4.2 when r_{m2} = 2.0(default), 1.5, 1.8, 2.5 and 3.0 in V5.0 in Yucheng. The correlation coefficient between SSA by V5.0 and V4.2 was the highest while setting r_{m2} as 2.0 (the default value) in V5.0 at the two sites.

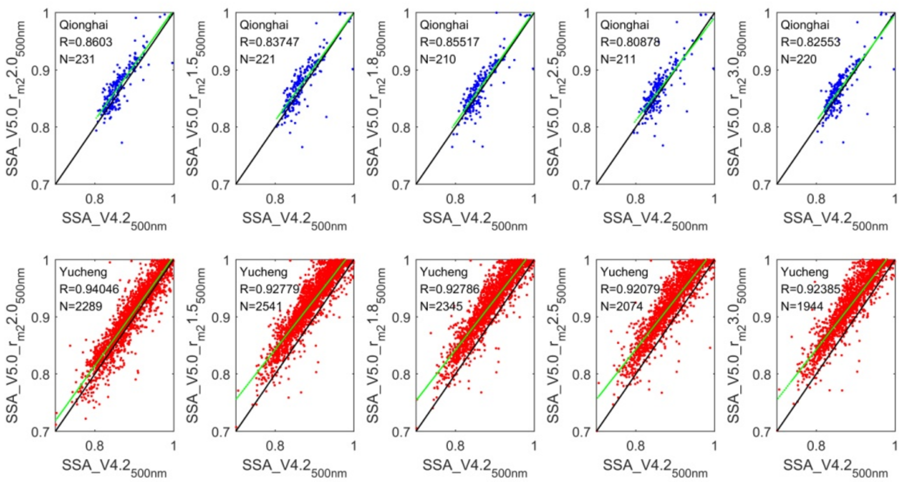

Figure 7: Scattergrams of retrieved SSA between SKYRAD V4.2 and V5.0 when r_{m2} =2.0(default), 1.5, 1.8, 2.5 and 3.0 for Qionghai (a) and Yucheng (b) in 2014.r_{m2} represents the model radius for the coarse mode SDF.

We also investigated whether the total amount of aerosols in the atmosphere were linked to the differences in SSA between the two versions. As shown in Fig. 8, the SSA differences at 500nm between the two versions (defined as: $|SSA\_V5.0_{500nm}$ - $SSA\_V4.2_{500nm}|$) decreased while the corresponding AODs at wavelengths of 500 nm by V5.0 increased at the two sites. When the AOD was high (in this study the threshold was set to 0.5 for AOD_{500nm}), SSA retrieved by V5.0 had a good comparison with those by V4.2. It is well known that the inversion products have a very high uncertainty in cases of very low aerosol burdens, the retrieval error in SSA rapidly increases with decreasing AOD, especially in parameters such as the imaginary part of the refractive index (Dubovik et al., 2000).

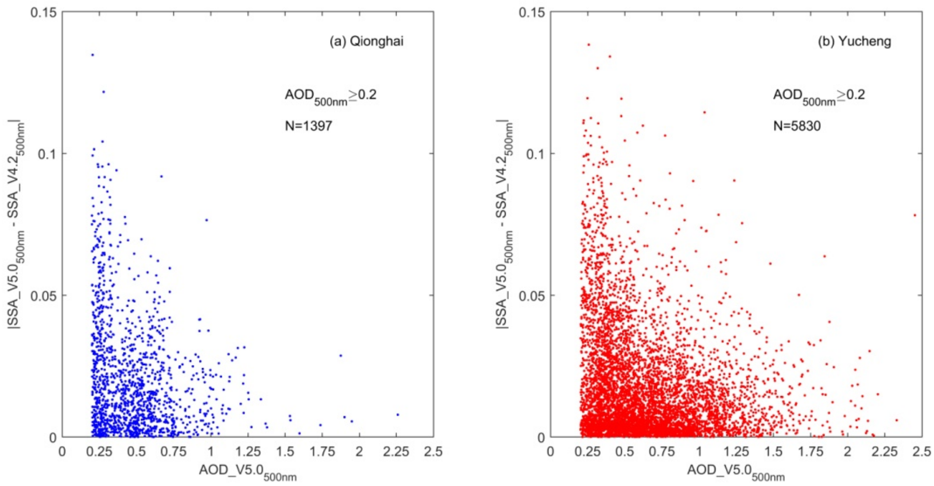

Figure 8: Scattergrams of the SSA differences at 500nm between V5.0 and V4.2 (defined as: |SSA_V5.0-SSA_V4.2|) and the corresponding AODs at wavelengths of 500 nm by V5.0 during February 2013 to December 2015.

Some tests by Hashimoto et al showed that the SDF setting in V5.0 was useful for detecting ill-conditioned data caused by cirrus contaminations, horizontally and/or temporally inhomogeneous aerosol stratification, and so on (Hashimoto et al., 2012).The SSA and m_i had high correlation coefficients between V4.2 and V5.0 with default r_{m2} value in V5.0 based on the above comparison results, we chose the retrieved results by V5.0 to analyze the seasonal variability of the aerosol optical properties over Qionghai and Yucheng in the following section.

3.2 Seasonal variability of the aerosol optical properties over Qionghai and Yucheng based on SKYRAD.pack V5.0

The analysis of the 500 nm channel was chosen because it was widely quoted in sun photometric and remote sensing applications and generally representative of visible band wavelengths (Estellés et al., 2012b). Four seasons were considered in this paper (i.e., spring (March–May), summer (June–August), autumn (September–November), and winter (December–February)) to investigate the seasonal variations of the aerosol optical properties over Qionghai and Yucheng based on SKYRAD.pack V5.0.

3.2.1The major chemical compositions in PM2.5 at the two sites

It is well known that OC, EC, $SO4^{2-}$, $NO3^{-}$ and $NH4^{+}$ were the dominant chemical components in PM2.5 (Tao et al., 2017). The above-mentioned five major components over the two sites were investigated based on the results simulated by the Community Multi-scale Air Quality model with the 2D Volatility Basis Set (CMAQ/2D-VBS) (23) at 36- × 36-km resolution with emission inputs derived from a Chinese emission inventory developed and updated to 2015, see details in these studies (Wang et al., 2014; Zhao et al., 2018). The contributors to carbonaceous aerosols in China mainly include coal combustion, vehicle exhaust and biomass burning, etc (Liu et al., 2018).As shown in Fig. 9, the concentrations of OC were significantly higher than that of EC at Qionghai, likely due to the mixed contributions of atmospheric chemical reactions and primary anthropogenic sources to OC (Cao et al., 2004). The nitrate accounted for a large fraction of PM2.5 in Yucheng, it was strongly related to the high emission levels of NH3 and O3 in Yucheng, especially in summer (Wen et al., 2015).

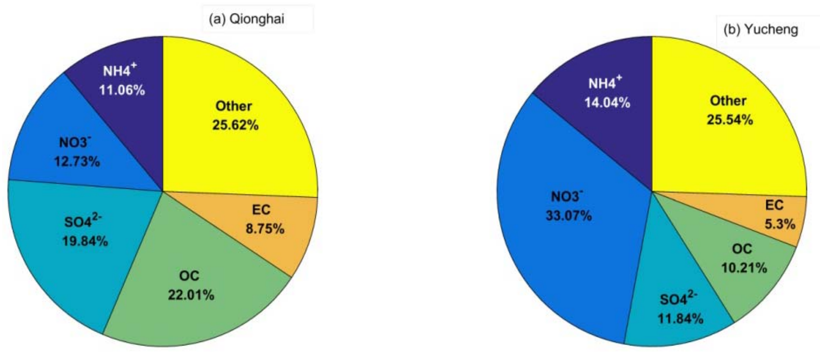

Figure 9: Percentage (%) contribution of $NO3^{-}$, $SO4^{2-}$,$NH4^{+}$,OC and EC to PM2.5 mass in Qionghai (a)and Yucheng (b) in 2015

3.2.2 AOD

The AOD is representative of the aerosol loading in the atmospheric column and important for the identification of the aerosol source regions and the aerosol evolution.

The AOD showed a distinct seasonal variation over both Qionghai and Yucheng. Figure 10a showed that the seasonal averaged AOD over Qionghai had higher values in spring, winter and autumn while lower in summer. During summer, the dominant wind is from South to Southeast (Zhu et al., 2005), the main emission source was from the South China Sea and West Pacific, in addition, seasonal upwelling off the east coast of Hainan Island was strongest in summer (Li et al., 2018) which was conducive to pollutant diffusion, meanwhile rich precipitation in summer was effective for eliminating aerosols, so seasonal averaged value of AOD in summer was the lowest in Qionghai, whereas AOD in spring was higher than other seasons. Southerly and northeasterly winds are both prevailing in spring over Qionghai (Liu et al., 2018), so long distance transport and emissions from surrounding areas were probably both the main pollutant sources.

The humidity in summer is the highest over Yucheng (Meng et al., 2007), the maximum AOD average of 0.99 occurring in summer maybe was caused by hygroscopic effects, high humidity combined with large fractions of hygroscopic chemical components (e.g. sulfate, nitrate, ammonium, and some organic matters) can enhance light extinction and haze intensity the scattering coefficient of secondary inorganic aerosols (such as sulfate, nitrate and ammonium) (Tao et al., 2017). The prevailing winds in Yucheng were from the northwest in winter and spring, and Yucheng was in the downwind of Hebei province where located many industrial enterprises emitted pollutants including secondary inorganic aerosols (Tao et al., 2017; Zhao et al., 2018c).AOD was higher in spring than in autumn and winter likely related to the long-range transportation of dust from northern/northwestern China and pollutants emitted from enterprises in Hebei (Tan et al., 2012; Tao et al., 2017).

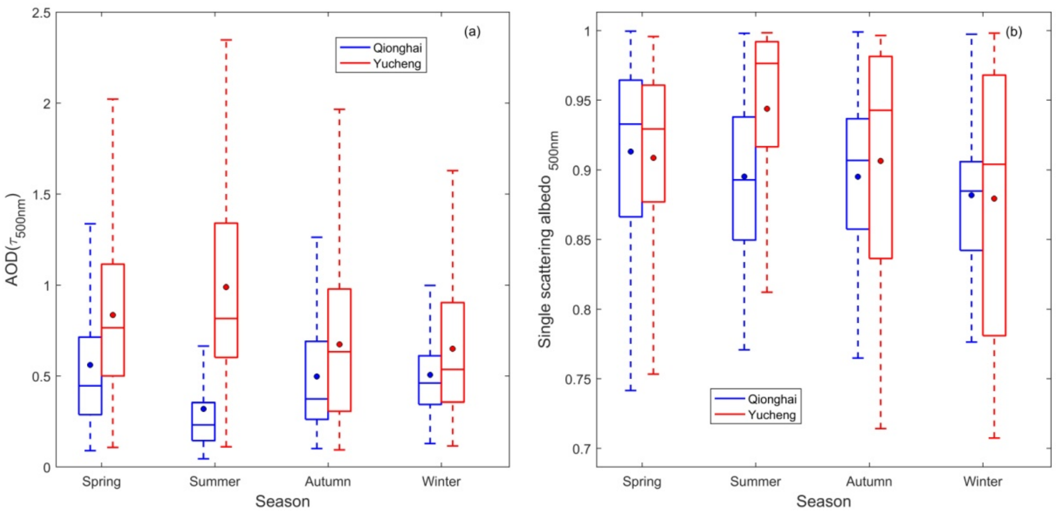

Figure 10: Seasonal variations in the AOD (a) and the single scattering albedo (SSA) (b) based on SKYRAD V5.0 over Qionghai and Yucheng for the period from February 2013 to December 2015. The boxes represent the 25th to 75th percentiles of the distributions while the dots and solid lines within each box represent the means and medians, respectively.

3.2.3 SSA

Figure 10b shows the seasonal averaged SSA at 500 nm for Qionghai and Yucheng during February

2013 to December 2015. The seasonal averaged SSA values were approximately 0.91, 0.90, 0.90, and 0.89 in spring, summer, autumn, and winter, respectively. The lowest seasonal average SSA was observed in winter, which was probably attributable to the regional transport of the air masses originated from the regions outside of Hainan province in Eastern China, where a great amount of coal was used for industrial enterprises and emitted high concentrations of OC and EC (Liu et al., 2018). In Yucheng, the seasonal pattern of SSA was consistent with AOD, the lowest seasonal average SSAs were also observed in winter due to carbonaceous aerosols increasing by heating activities and biomass burning, seasonal average contributions of carbonaceous aerosols were evidently higher in cold seasons than in warm seasons (Tao et al., 2017). High concentrations of fine particulate nitrate were frequently observed in summer in Yucheng (Wen et al., 2015), likely to cause the high SSA in summer.

3.2.4Volume Size Distribution

Figures 11a and b show the seasonal averaged volumes of the different aerosol particle size distributions (d**v**/dln*r*) in Qionghai and Yucheng. The aerosol volume size distributions were typical bimodal patterns during each season at the Qionghai and Yucheng sites. Figures 11a and 11b show that there was a larger contribution of coarse-mode particles to the aerosol volume compared with the fine-mode particles at the two sites. The fine mode showed a peak at a radius of 0.17 μm in all seasons over Qionghai. The coarse mode was characterized by a peak at a radius of 5.29 μm in spring, summer, and autumn and 3.62 μm in winter. As shown in Fig. 11a, the fraction of the fine aerosol particles was much smaller in summer than other seasons, the summer meteorological conditions such as high wind speeds, high mixing heights, and the fresh air masses originated from or passed through the sea, which may be contributable to the decrease of anthropogenic pollutant concentrations (Liu et al., 2018) and introducing some sea salt particles of a relatively large size. The seasonal averaged peak of fine mode and coarse mode SDF were both higher in winter than other seasons as shown in Fig.11a. The stable atmospheric circulation provides a stable atmospheric environment background, which is not conducive to the diffusion of pollutants; moreover, continuous low-level northeast wind facilitates the transportation of pollutants from the inland to Hainan in winter (Wu et al., 2011; Liu et al., 2018).

As shown in Fig. 11b, the coarse-mode particle in Yucheng had a relatively large value compared to the volume distribution of the fine-mode particle. The aerosol was not only from winter heating but also from regional transport in winter (Tao et al., 2017; Zhao et al., 2018c). The volume of the coarse aerosol particles relative to the whole was much larger in spring than other seasons in Yucheng probably because of the presence of the dust particles transported from the northwest of China and pollutants emitted from enterprises in Hebei (Tao et al., 2017).

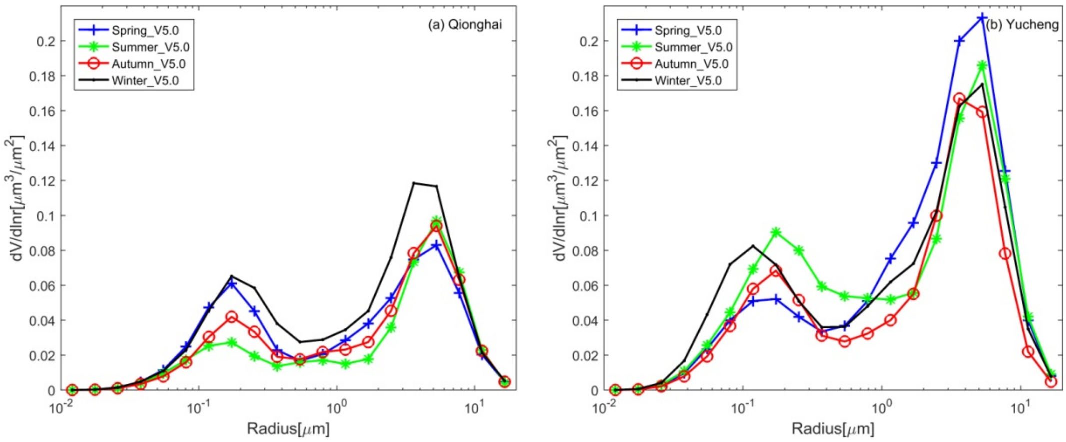

Figure 11: Seasonally averaged volumes of the different aerosol particle size distributions based on SKYRAD V5.0 over Qionghai (a) and Yucheng (b) for the period from February 2013 to December 2015.

3.2.5 Refractive index

The real part of the refractive index (m_r) represents scattering. A higher m_r indicates a higher scattering. The imaginary part of the refractive index (m_i) represents absorption of the aerosols and is an important quantity in evaluating the aerosol radiative forcing.

Figure 12a showed the seasonal variation of the real part of the refractive index (m_r) at 500 nm over Qionghai and Yucheng. The seasonal averages of m_r at 500 nm were 1.45, 1.46, 1.45, and 1.43 in spring, summer, autumn, and winter in Qionghai, respectively. The m_r showed a maximum of approximately 1.47 in spring and a minimum of approximately 1.45 in summer in Yucheng. Figure 12b presented the seasonal variation of the imaginary part of the refractive index at 500 nm over Qionghai and Yucheng. The results of imaginary part of complex refractive index (m_i) were both the highest in winter over the two sites. Aerosol absorption coefficient was mainly determined by elemental carbon (EC) mass concentration and its coating (Tao et al., 2017), heating activities and biomass burning induced higher carbonaceous aerosols in winter in Yucheng. As shown in Fig.9, OC/EC ratios could be estimated to be greater than 2.0 in Qionghai, suggesting coal and vehicle exhaust as dominant carbonaceous aerosols sources (He et al., 2008; Watson et al., 2001).

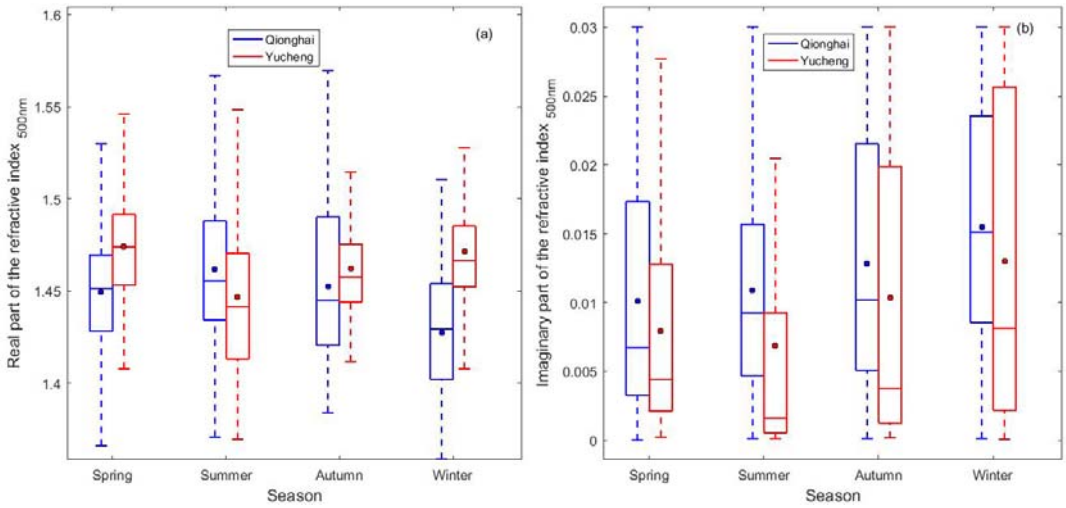

Figure 12: Seasonal variations in the real part of the refractive index (a) and the imaginary part of the refractive index (b) based on SKYRAD V5.0 over Qionghai and Yucheng for the period from February 2013 to December 2015. The boxes represent the 25th to 75th percentiles of the distributions while the dots and solid lines within each box represent the means and medians, respectively.

4 Summary

The aerosol optical properties over the two new SKYNET sites of Qionghai and Yucheng in China were continuously investigated over two years using the RREDE-POM02 sky radiometer measurements. As V5.0 used an a priori SDF of a bimodal log-normal function, the volume size distribution retrieved by V5.0 presented an overall bimodal pattern with a 0.10-0.20 μm fine particle mode and a 3.0–6.0 μm coarse particle mode both over Qionghai and Yucheng. The correlation coefficients between SSAs by V5.0 and by V4.2 were around 0.88, 0.87, 0.90, 0.88 and 0.92 at wavelengths of 400, 500, 670, 870, and 1020 nm over Qionghai, respectively. The SSA values computed from V5.0 had relatively high correlation coefficients with R= 0.95, 0.95, 0.96, 0.94, 0.91 at wavelengths of 400, 500, 670, 870, and 1020 nm in Yucheng. The correlation coefficients between m_i by V5.0 and those by V4.2 at the five wavelengths were all higher than 0.89 over Yucheng.

Sensitivity tests showed that the correlation coefficient between SSAs at 500nm by V5.0 and V4.2 was higher while setting r_{m2} as 2.0μm (the default value) in V5.0 than r_{m2} = 1.5, 1.8, 2.5 and 3.0 μm at the two sites. The SSA differences at 500nm between the two versions decreased with the increase of the corresponding AODs at the two sites.

Based on SKYRAD.pack V5.0, the seasonal variations of the aerosol optical properties over Qionghai and Yucheng were investigated. The seasonal patterns of AOD were quite different between the two stations. The AOD showed high values in spring, autumn and winter but decreased to minimum in summer over Qionghai, likely related to summer monsoon from the South China Sea and West Pacific that brought most of the annual rainfall to the island, whereas the winter monsoon from Inner Mongolia carried the air masses from the mainland China to Qionghai. In Yucheng, the maximum seasonal averaged AOD and SSA both appeared in summer due to the hygroscopic effects. The fraction of the fine aerosol particles over Qionghai was much smaller in summer probably related to wet deposition, more precipitation in the summer can lead to more efficient removal of aerosol. The volume of the coarse aerosol particles relative to the whole in spring was much larger than other seasons in Yucheng, probably due to the presence of the dust particles transported from the northwest of China and pollutants emitted from enterprises in Hebei. The location and distribution of major industrial sources, intensity of local minor sources such as winter heating, and prevailing wind directions together caused the different magnitudes of seasonal variations among the two sites discussed above.

The comparison results between the aerosol optical properties retrieved by SKYRAD5.0 and SKYRAD4.2 were very different over the two SKYNET sites. The results can provide validation data in China for SKYNET to continue improving data-processing and inversion method. Meanwhile, the results can promote the integration of more Chinese observation stations into international network.

Data availability. The sky radiometer data at Qionghai and Yucheng, China are available on request by contacting the first author of the paper (jiangzhe@mail.iap.ac.cn).

Author contributions. Zhe Jiang and Huizheng Che designed the present study, Minzheng Duan and Wenxing Zhang performed observation, Zhe Jiang analyzed data and wrote the paper, with support from all the authors. Teruyuki Nakajima designed the inversion method and Makiko Hashimoto improved the inversion method. Teruyuki Nakajima, Makiko Hashimoto, Bin Chen and Akihiro Yamazaki gave useful comments.

Competing interests. The authors declare that they have no conflict of interest.

Acknowledgements. This work was supported by the National Key Research and Development Program of China (2017YFB0503603) and the National Natural Science Foundation of China (41975178, 41825011, 41301381, 41475026 and 41705014).

References

Ackerman, A. S., Toon, O. B., Stevens, D. E., Heymsfield, A.J., Ramanathan, V., and Welton E.J.:

Reduction of tropical cloudiness by soot, Science, 288, 1042–1047, doi: 10.1126/science.288.5468.1042, 2000.

Bi, J. R., Shi, J. S. , Xie, Y. K., and Liu Y. Z.: Dust Aerosol Characteristics and Shortwave Radiative Impact at a Gobi Desert of Northwest China during the Spring of 2012, J. Meteor. Soc. Japan, 92A, 33–56, doi: 10.2151/jmsj.2014-A03, 2014.

Cai J. X., Guan, Z. Y. , and Ma, F. H. : Possible combined influences of absorbing aerosols and anomalous atmospheric circulation on summertime diurnal temperature range variation over the middle and lower reaches of the Yangtze River, J. Meteor. Res., 30(6), 927–943,doi: 10.1007/s13351-016-6006-1, 2016.

Campanelli, M., Nakajima, T., and Olivieri, B.: Determination of the solar calibration constant for a sun-sky radiometer: Proposal of an in-situ procedure, Appl. Opt., 43, 651–659, doi:10.1364/AO.43.000651, 2004.

Campanelli, M., Lupi, A., Nakajima, T., Malvestuto, V., Tomasi, C., and Estelles, V.: Summertime columnar content of atmospheric water vapor from ground-based Sun-sky radiometer measurements through a new in situ procedure, J. Geophys. Res., 115, D19304, doi:10.1029/2009JD013211, 2010.

Che, H., Shi, G., Uchiyama, A., Yamazaki, A., Chen, H., Goloub, P., and Zhang, X.: Intercomparison between aerosol optical properties by a PREDE skyradiometer and CIMEL sunphotometer over Beijing, China, Atmos. Chem. Phys., 8, 3199–3214, doi:10.5194/acp-8-3199-2008, 2008.

Che, H. Z., Xia, X. A., Zhu, J., Wang, H., Wang, Y. Q., Sun, J.Y., Zhang, X. C., Zhang, X. Y., and Shi, G. Y.: Aerosol optical properties under the condition of heavy haze over anurban site of Beijing, China, Environ. Sci. Pollut. R., 22, 1043–1053, https://doi.org/10.1007/s11356-014-3415-5, 2014.

Che, H. Z., Qi, B., Zhao, H. J., Xia, X. A., Eck, T. F., Goloub, P., Dubovik, O., Estelles, V., Cuevas-Agulló, E., Blarel, L., Wu, Y. F., Zhu, J., Du, R. G., Wang, Y. Q., Wang, H., Gui, K., Yu, J., Zheng, Y., Sun, T. Z., Chen, Q. L., Shi, G. Y., and Zhang, X. Y..: Aerosol optical properties and direct radiative forcing based on measurements from the China Aerosol Remote Sensing Network (CARSNET) in eastern China, Atmos. Chem. Phys., 18, 405–425, doi:10.5194/acp-18-405-2018, 2018.

Chen, Z., Lu, C. and Fan, L.: Farmland changes and the driving forces in Yucheng, North China Plain. Journal of Geographical Sciences, 22(3), 563-573, 2012.

Dusek, U., Frank, G. P., Hildebrandt, L., Curtius, J., Schneider, J., Walter, S., Chand, D., Drewnick, F., Hings, S., Jung, D., Borrmann, S., and Andreae, M. O.: Size matters more than chemistry for cloud-nucleating ability of aerosol particles, Science, 312(5778), 1375–1378, doi:10.1126/science.1125261, 2006.

Estellés, V., Campanelli, M., Utrillas, M. P., Expósito, F., and Martínez-Lozano, J. A.: Comparison of AERONET and SKYRAD4.2 inversion products retrieved from a Cimel CE318 sunphotometer, Atmos. Meas. Tech., 5, 569–579, https://doi.org/10.5194/amt-5-569-2012, 2012a.

Estellés, V., Smyth, T. J., Campanelli, M.: Columnar aerosol properties in a Northeastern Atlantic site (Plymouth,United Kingdom) by means of ground based skyradiometer data during years 2000-2008, Atmos. Environ., 61, 180–188, doi :10.1016/j.atmosenv.2012.07.024, 2012b.

Hashimoto, M., Nakajima, T., Dubovik, O., Campanelli, M., Che, H., Khatri, P., Takamura, T., and Pandithurai, G.: Development of a new data-processing method for SKYNET sky radiometer observations, Atmos. Meas. Tech., 5, 2723–2737, https://doi.org/10.5194/amt-5-2723-2012, 2012.

He, L. Y., Hu, M., Zhang, Y. H., Huang, X. F., and Yao, T. T.: Fine particle emissions from on-road vehicles in the Zhujiang Tunnel, China, Environmental Science & Technology, 42, 4461-4466, 2008.

Hensen, J., Sato, M., and Ruedy, R.: Radiative forcing and climate response, J. Geophys. Res., **102**(D6), 6831‒6864, doi:10.1029/96JD03436, 1997.

Higurashi, A., Nakajima, T., Holben, B., Smirnov, A., Frouin, R., and Chatenet, B.: A study of global aerosol optical climatology with two channel AVHRR remote sensing, J. Climate, 13, 2011–2027, 2000.

Kaufman, Y. J., Koren, I., Remer, L. A., Rosenfeld, D., and Rudich, Y.: The effect of smoke, dust, and pollution aerosol on shallow cloud development over the Atlantic Ocean, Proc. Natl. Acad. Sci. U.S.A., 102, 11207–11212, doi: 10.1073/pnas.0505191102, 2005.

Kim, D. H., Sohn, B. J., Nakajima, T., Takamura, T., Takemura, T., Choi, B. C., and Yoon, S. C.: Aerosol optical properties over east Asia determined from ground-based sky radiation measurements, J. Geophys. Res., 109, D02209, doi:10.1029/2003JD003387, 2004.

Li, M., Xie, L., Zong, X., Zhang, S., Zhou, L., and Li, J.: The cruise observation of turbulent mixing in the upwelling region east of Hainan Island in the summer of 2012. Acta Oceanologica Sinica, 37(9), 1-12, 2018.

Liu, B., Zhang, J., Wang, L., Liang, D., Cheng, Y., Wu, J., Bi, X., Feng, Y., Zhang, Y., and Yang, H.:Characteristics and sources of the fine carbonaceous aerosols in Haikou, China. Atmospheric Research, 199, 103-112, 2018.

Lu, W., Yang, L., Chen, J., Wang, X., Li, H., Zhu, Y., Wen, L., Xu, C., Zhang, J., Zhu, T. and Wang, W.: Identification of concentrations and sources of PM 2.5-bound PAHs in North China during haze episodes in 2013. Air Quality, Atmosphere & Health, 9(7), 823-833, 2016.

Meng, C. L., and Xu, Z. X.: Relation between ENSO and Precipitation in Shandong . Yellow River, 1, 2007 (in Chinese).

Nakajima, T., Tanaka, M., and Yamauchi, T.: Retrieval of the optical properties of aerosols from the aureole and extinction data, Appl. Optics, 22, 2951–2959, doi: 10.1364/AO.22.002951, 1983.

Nakajima, T. and Tanaka, M.: Algorithms for radiative intensity calculations in moderately thick atmospheres using a truncation approximation, J. Quant. Spectrosc. Ra., 40, 51–69, doi: 10.1016/0022-4073(88)90031-3, 1988.

Nakajima, T., Tonna, G., Rao, R., Kaufman, Y., and Holben, B.: Use of sky brightness measurements from ground for remote sensing of particulate polydispersions. Appl. Optics, 35, 2672–2686, doi: 10.1364/AO.35.002672, 1996.

Nakajima, T., Yoon, S. C., Ramanathan, V., Shi, G. Y., Takemura, T., Higurashi, A., Takamura, T., Aoki, K., Sohn, B. J., Kim, S. W., Tsuruta, H., Sugimoto, N., Shimizu, A., Tanimoto, H., Sawa, Y., Lin, N. H., Lee, C. T., Goto, D., and Schutgens, N.: Overview of the Atmospheric Brown Cloud East Asian Regional Experiment 2005 and a study of the aerosol direct radiative forcing in east Asia, J. Geophys. Res., 112, D24S91, doi:10.1029/2007JD009009, 2007.

Peel, M. C. and Finlayson, B. L. and McMahon, T. A.: Updated Asian map of the Köppen climate classification system. Hydrol. Earth Syst. Sci. 11: 1633-1644, 2007.

Phillips, B. L.: A technique for numerical solution of certain integral equation of first kind, J. Assoc. Comput. Mach., 9, 84–97, 1962.

Pope Iii, C.A., Burnett, R.T., Thun, M. J., Calle, E. E., Krewski, D., Ito, K., and Thurston, G. D.: Lung cancer, cardiopulmonary mortality, and long-term exposure to fine particulate air pollution, J. Am. Med. Assoc, 287(9), 1132–1141, doi: 10.1001/jama.287.9.1132, 2002.

Ramanathan, V., Crutzen, P. J., Kiehl, J. T., Rosenfeld, D.: Aerosols, climate, and the hydrological cycle, Science, 294, 2119–2124, 2001.

Rodgers, C. D.: Inverse Method for Atmospheric Sounding, World Sci., Singapore, 240, 2000.

Samet, J.M., Zeger, S.L., Dominici, F., Coursac, I., Dockery, D.W., Schwartz, J., and Zanobetti, A.: The national morbidity, mortality, and air pollution study. Part II: morbidity and mortality from air pollution in the United States, Health Effects Institute, Cambridge MA, Research Report 94, 2000.

Sun, K., Liu, H. N., Wang, X. Y., Peng, Z., and Xiong, Z.: The aerosol radiative effect on a severe haze episode in the Yangtze River Delta., J. Meteor. Res., 31(5), 865–873, doi: 10.1007/s13351-017-7007-4, 2017.

Takamura, T., and Nakajima, T.: Overview of SKYNET and its activities, Opt. Pura Y Apl., 37, 3303–3308, 2004.

Tan, S. C., Shi, G. Y., and Wang, H.: Long-range transport of spring dust storms in Inner Mongolia and impact on the China seas. Atmospheric Environment, 46, 299-308, 2012.

Tang, J.X., Fu, C. B., Dan, L., Lin X. B.: Analysis on potential sources of air pollutants in Hainan during haze pollution. Environmental Science and Management, 06, 2019 (in Chinese).

Tao, J., Zhang, L., Cao, J., and Zhang, R.:A review of current knowledge concerning PM 2. 5 chemical composition, aerosol optical properties and their relationships across China. Atmospheric Chemistry and Physics, 17(15), 9485-9518, 2017.

Twomey, S.: On the numerical solution of Fredholm integral equations of the first kind by the inversion of the linear system produced by quadrature, J. Assoc. Comput. Mach., 10, 97–101, 1963.

Turchin, V. F. and Nozik, V. Z. : Statistical regularization of the solution of incorrectly posed problems, Izv. Atmos. Ocean. Phy.+, **5**, 14–18, 1969.

Uchiyama, A., Yamazaki, A., Togawa, H., and Asano, J.: Characteristics of Aeolian dust observed by sky-radiometer in the Intensive Observation Period 1 (IOP1), J. Meteor. Soc. Japan, 83A, 291–305, doi: 10.2151/jmsj.83A.291, 2005.

Wang, S. X., Zhao, B., Cai, S. Y., Klimont, Z., Nielsen, C. P., Morikawa, T., Woo, J. H., Kim, Y., Fu, X., Xu, J. Y., Hao, J. M., and He, K. B.: Emission trends and mitigation options for air pollutants in East Asia. Atmospheric Chemistry and Physics, 14(13), 6571-6603, 2014.

Wang, Z. W., Yang, S. Q., Zeng, Q. L., and Wang, Y. Q.: Retrieval of aerosol optical depth for Chongqing using the HJ-1 satellite data, J. Meteor. Res., 31(3), 586 – 596, doi: 10.1007/s13351-017-6102-x, 2017.

Wang, Z. Z., Liu, D., Wang, Z., Wang, Y. J., and Khatri, P.: Seasonal characteristics of aerosol optical properties at the SKYNET Hefei site (31.90°N, 117.17°E) from 2007 to 2013, J. Geophys. Res., 119, 6128–6139, doi:10.1002/2014JD021500, 2014.

Wen, L., Chen, J.M., Yang, L.X., Wang, X.F., Xu, C.H., Sui, X., Yao, L., Zhu, Y.H., Zhang, J.M., Zhu, T., and Wang, W.X.: Enhanced formation of fine particulate nitrate at a rural site on the North China Plain in summer: The important roles of ammonia and ozone, Atmospheric Environment, 101, 294-302, 2015.

Wu, D., Wu, C., Li, F., and Chen, H.: Air pollution episode in southern China due to the long range transport of coarse particle aerosol. China Environmental Science, 31(4), 540-545, 2011(in Chinese).

Yang, Y. R., Liu, X. G., Qu, Y., An, J. L., Jiang, R., Zhang, Y. H., Sun, Y. L., Wu, Z. J., Zhang, F., Xu, W. Q., and Ma, Q. X.: Characteristics and formation mechanism of continuous hazes in China: A case study during the autumn of 2014 in the North China Plain, Atmos.Chem. Phys., 15, 8165-8178, doi: 10.5194/acp-15-8165-2015, 2015.

Yin, Y., Zhu, D., Tang, W.W., Martini I. P.: The application of GPR to barrier-lagoon sedimentation study in Boao of Hainan Island. Journal of Geographical Sciences, 12(3), 313-320, 2002.

Zhao, B., Wang, P., Ma, J.Z., Zhu, S., Pozzer, A., and Li, W.: A high-resolution emission inventory of primary pollutants for the Huabei region, China. Atmos.Chem. Phys., 12, 481-501, 2012.

Zhao, B., Liou, K.-N., Gu, Y., Jiang, J. H., Li, Q., Fu, R., Huang, L., Liu, X., Shi, X., Su, H., and He, C.: Impact of aerosols on ice crystal size, Atmos. Chem. Phys., 18, 1065-1078, DOI 10.5194/acp-18-1065-2018, 2018a.

Zhao, B., Zheng, H., Wang, S., Smith, K. R., Lu, X., Aunan, K., Gu, Y., Wang, Y., Ding, D., Xing, J., Fu, X., Yang, X. D., Liou, K. N., and Hao, J.M.: Change in household fuels dominates the decrease in PM2. 5 exposure and premature mortality in China in 2005–2015. Proceedings of the National Academy of Sciences, 115(49), 12401-12406, 2018b.

Zhao, B., Jiang, J. H., Diner, D. J., Su, H., Gu, Y., Liou, K.-N., Jiang, Z., Huang, L., Takano, Y., Fan, X.H., and Omar, A. H.: Intra-annual variations of regional aerosol optical depth, vertical distribution, and particle types from multiple satellite and ground-based observational datasets, Atmos. Chem. Phys., 18, 11247–11260, doi:10.5194/acp-18-11247-2018, 2018c.

Zhu, D., Yin, Y., Martini, I. P.: Geomorphology of the Boao coastal system and potential effects of human activities - Hainan Island, South China. Journal of Geographical Sciences, 15(2):187-198, 2005.

Table 1. Averaged single scattering albedo and refractive index in SKYRAD 5.0 and 4.2, and the absolute and percentage differences between the two versions at Qionghai site during February 2013 to December 2015.

	400 nm	500 nm	670 nm	870 nm	1020 nm
$\omega_{v5.0}$	0.8649	0.9053	0.9305	0.9439	0.8803
$\omega_{v4.2}$	0.8834	0.9183	0.9426	0.9582	0.8760
$m_{r\_v5.0}$	1.4549	1.4423	1.4322	1.4414	1.4897
$m_{r\_v4.2}$	1.4260	1.4398	1.4482	1.4650	1.4623
$m_{i\_v5.0}$	0.0029	0.0018	0.0013	0.0011	0.0026
$m_{i\_v4.2}$	0.0025	0.0016	0.0010	0.0007	0.0025
$\delta\omega$	-0.0185	-0.0130	-0.0121	-0.0143	0.0043
δm_r	0.0289	0.0024	-0.0159	-0.0236	0.0274
δm_i	0.0004	0.0002	0.0003	0.0004	0.0001
$\delta\omega\%$	-0.0210	-0.0141	-0.0128	-0.0149	0.0049
$\delta m_{r\%}$	0.0203	0.0017	-0.0110	-0.0161	0.0187
R_{mi}	1.1865	1.1341	1.2679	1.6558	1.0155

ω, m_r and m_i mean averaged single scattering albedo, real part of refractive index and the imaginary part of refractive index; subscript v5.0 and v4.2 mean parameters retrieved by SKYRAD V5.0 and V4.2, respectively; δ- and δ-% mean absolute and percentage difference between SKYRAD V5.0 and V4.2, respectively; R_{mi} means the ratio of $m_{i\_v5.0}$ to $m_{i\_v4.2}$.

Table 2. The same as Table 1 but for Yucheng during February 2013 to December 2015.

	400 nm	500 nm	670 nm	870 nm	1020 nm
$\omega_{v5.0}$	0.8737	0.9131	0.9158	0.9243	0.8918
$\omega_{v4.2}$	0.9044	0.9250	0.9394	0.9543	0.9264
$m_{r\_v5.0}$	1.4466	1.4521	1.4743	1.5251	1.5522
$m_{r\_v4.2}$	1.4970	1.5053	1.5080	1.5380	1.5333
$m_{i\_v5.0}$	0.0032	0.0021	0.0023	0.0023	0.0032
$m_{i\_v4.2}$	0.0029	0.0023	0.0019	0.0015	0.0028
$\delta\omega$	-0.0306	-0.0119	-0.0237	-0.0299	-0.0346
δm_r	-0.0504	-0.0532	-0.0337	-0.0129	0.0188
δm_i	0.0003	-0.0002	0.0004	0.0008	0.0004
$\delta\omega\%$	-0.0339	-0.0129	-0.0252	-0.0314	-0.0373
$\delta m_{r\%}$	-0.0337	-0.0353	-0.0224	-0.0084	0.0123
R_{mi}	1.1192	0.9505	1.2016	1.4931	1.1308

ω, m_r and m_i mean averaged single scattering albedo, real part of refractive index and the imaginary part of refractive index; subscript v5.0 and v4.2 mean parameters retrieved by SKYRAD V5.0 and V4.2, respectively; δ- and δ-% mean absolute and percentage difference between SKYRAD V5.0 and V4.2, respectively; R_{mi} means the ratio of $m_{i\_v5.0}$ to $m_{i\_v4.2}$.